Supplementary Information

Unveiling the Dynamics of Urbanization and Ecosystem Services: Insights from the Su-Xi-Chang Region, China

Supplementary Notes

Supplementary Note 1

It is worth noting that waters have undergone complex changes due to the dual influence of natural and anthropogenic factors. First, the expansion of built-up area in developing urban areas came from cultivated land and waters. Human activities intensified between 1990 and 2020, especially in developing urban areas. The booming economy and population may have facilitated land reclamation, increasing the conversion rate of lakes to cultivated land and built-up land. Second, the main land use change in the rural areas is the conversion of cropland to waters. On the one hand, this may be closely related to China's policy of "returning farmland to lakes", which helps to maintain regional ecosystem balance[1]. On the other hand, the gradual increase in precipitation may also be an important factor influencing the expansion of the lake area and the rise in its water level[2].

Supplementary Table 1. Quantitative changes in different land-use types from 1990 to 2020.

Urbanization level areas	Year	Cultivated land	Forest	Grassland	Water area	Built-up area	Unused land
The whole study area	1990	11873.3	876.7	2.8	4064.5	854.3	0.2
	2000	10714.2	895.3	0.7	4422.9	1638.6	0.1
	2010	8883.7	827.4	9.4	4651.6	3299.4	0.2
	2020	8420.8	756.7	0.2	4179.1	4314.5	0.3
Developed urban area	1990	80.9	6.2	0.0	13.0	129.9	0.0
	2000	33.5	5.9	0.0	11.2	179.4	0.0
	2010	10.8	5.1	0.0	10.9	203.2	0.0
	2020	8.9	4.7	0.0	11.1	205.3	0.0
Developing urban area	1990	6804.2	157.2	1.6	835.6	525.1	0.0
	2000	6079.7	157.1	0.4	980.4	1106.1	0.0
	2010	4643.8	142.2	8.2	995.3	2534.1	0.2
	2020	4061.2	121.5	0.1	790.7	3349.9	0.3
Rural area	1990	4896.8	679.1	1.1	3147.1	197.4	0.1
	2000	4512.8	698.6	0.2	3360.9	349.1	0.0
	2010	4151.6	647.5	1.1	3571.3	550.1	0.0
	2020	4274.5	598.6	0.1	3305.9	742.6	0.0

Note: Land was divided into six categories: cultivated land, forest, grassland, water area, built-up area and unused land (Unit: km^2).

Supplementary Note 2

In general, various ESs in the Su-Xi-Chang region showed significant spatial heterogeneity (Supplementary Figure 1). The high-value areas of GP were concentrated in the west and northeast of the study area, with a large and relatively flat cultivated land (Supplementary Figure 1a). The high value areas of WR (Supplementary Figure 1b) and FM (Supplementary Figure 1d) were concentrated in the relatively higher elevation forest in the southwest of the study area and around Taihu Lake. The high value areas of HM were concentrated in the western part of the study area and around Taihu Lake (Supplementary Figure 1c). The low value areas of the four ESs were mainly concentrated in the urban core areas of Suzhou, Wuxi and Changzhou and their surroundings.

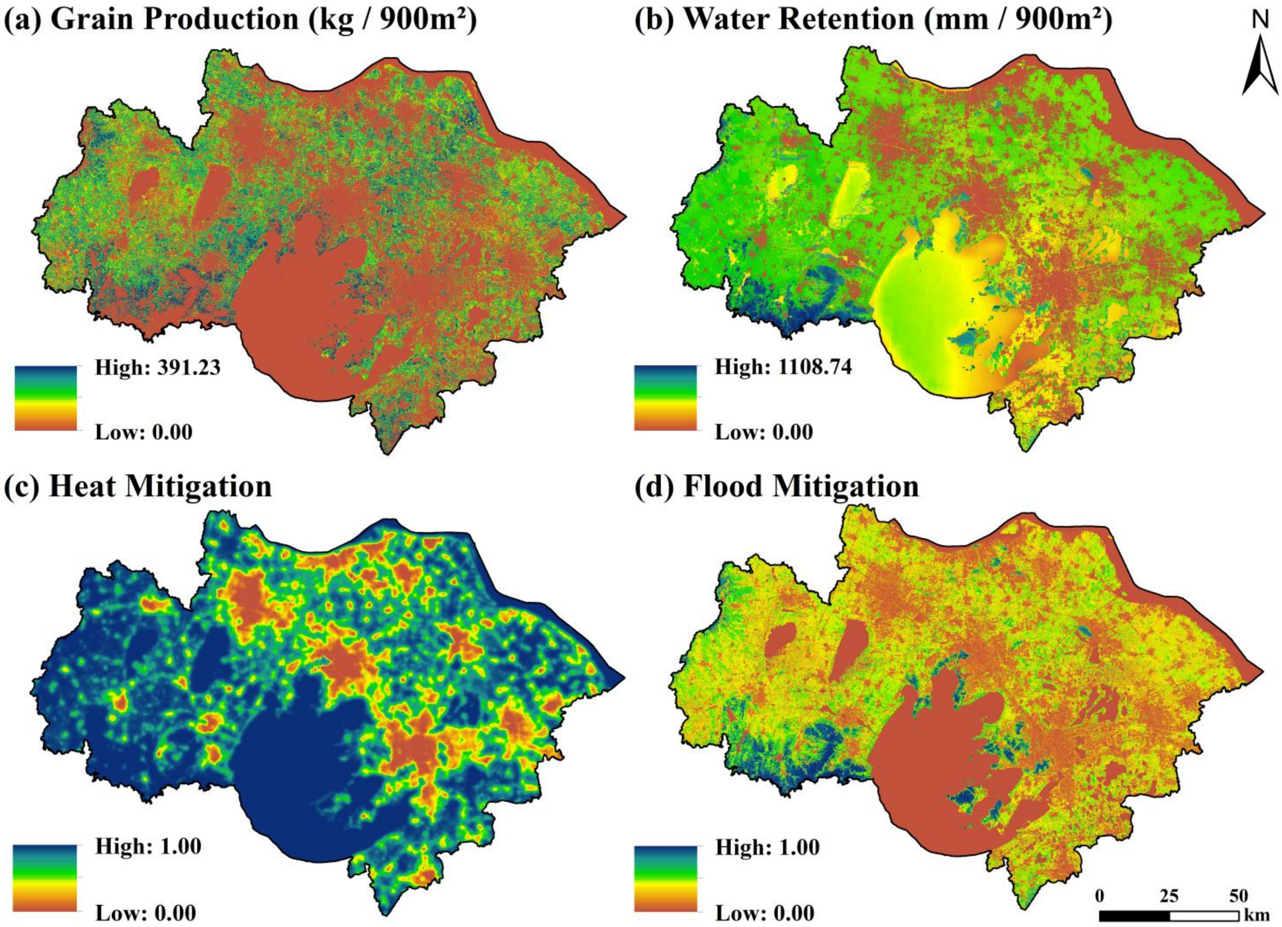

Supplementary Figure 1. Spatial distribution pattern of ESs in 2020. (a) grain production; (b) water retention; (c) heat mitigation; (d) flood mitigation.

In general, the mean values of the four ESs in different urbanization areas were as follows: rural area > developing urban area > developed urban area (Supplementary Figure 2). GP was similar in the developing urban area and rural area with 0.117 kg m^-2 and

0.123 kg m^-2, respectively. GP in the developed urban area was the lowest, at 0.0095 kg m^-2 (Supplementary Figure 2a). WR was the highest in the rural area with 0.449 mm m^-2. This was followed by the developing urban area with an average of 0.276 mm m^-2. The lowest was in the developed urban area with 0.048 mm m^-2 (Supplementary Figure 2b). The mean values of HM in the developed urban areas, developing urban areas and rural areas were 0.14, 0.6 and 0.92, respectively (Supplementary Figure 2c). The mean values of FM in the developed urban areas, developing urban areas and rural areas were 0.07, 0.15 and 0.17, respectively (Supplementary Figure 2d).

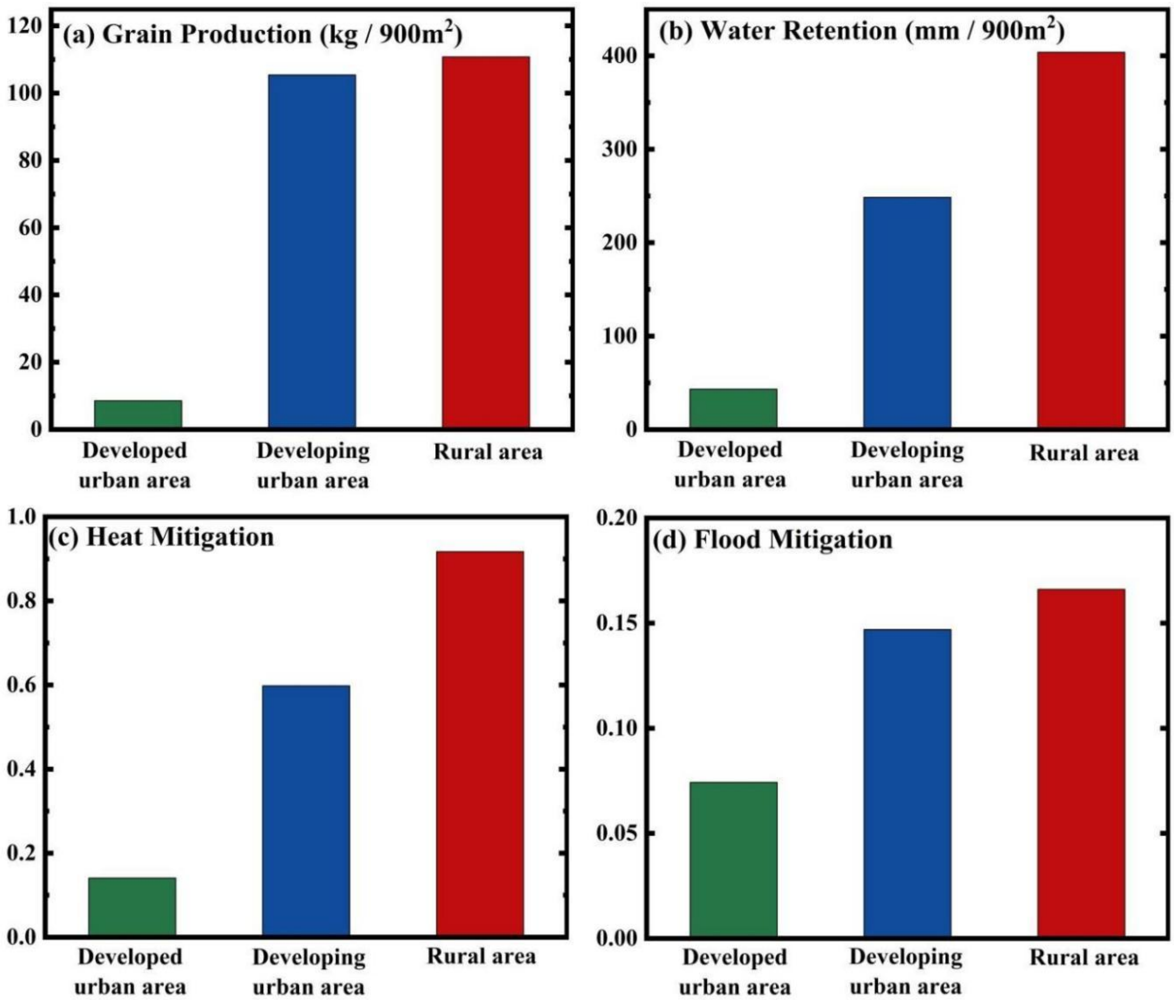

Supplementary Figure 2. Average values of the ESs in the different urbanization areas in 2020. (a) grain production; (b) water retention; (c) heat mitigation; (d) flood mitigation.

Supplementary Methods

Supplementary Method 1

Grain Production. Grains in this study refer to wheat, late-season rice, potatoes, soybean, and broad and pea bean. Recent studies have shown that normalized difference vegetation index (*NDVI)* can better estimate grain yields such as wheat[3], soybean[4], and rice yield[5].

Referring to the method of Liu et al.[6], we used *NDVI* data to calculate the vegetation condition index *(VCI)* of the ith cultivated land pixel, and allocated the total grain yield to each cultivated land pixel. The calculation formula are as follows.

$$\mathrm{GP_i} = \mathrm{GP_y} \times \frac{\mathrm{VCI_i}}{\sum_{\mathrm{i=1}}^{a} \mathrm{VCI_i}} \tag{1}$$

$$\mathrm{VCI_i} = \frac{(\mathrm{NDVI_i} - \mathrm{NDVI_{min}})}{\mathrm{NDVI_{max}} - \mathrm{NDVI_{min}}} \times 100\% \tag{2}$$

Among them, $\mathrm{GP_i}$ is the grain yield of the ith cultivated land pixel, kg; $\mathrm{GP_y}$ is the total grain yield over the years, kg; *a* is the total number of pixels of the cultivated land; $\mathrm{NDVI_i}$ is the annual *NDVI* value of the ith cultivated land pixel; $\mathrm{NDVI_{max}}$ and $\mathrm{NDVI_{min}}$ represent the maximum and minimum annual *NDVI* values of the cultivated land, respectively.

Water Retention. We adopted the method of Bai et al.[7] to calculate WR according to the difference between water yield and surface runoff. Water yield was calculated using the Water Yield module of the InVEST model. The calculation formula are as follows.

$$\mathrm{WR_{ij}} = \mathrm{WY_{ij}} - \mathrm{RF_{ij}} \tag{3}$$

$$\mathrm{RF_{ij}} = \mathrm{P_i} \times \mathrm{C_{ij}} \tag{4}$$

$$\mathrm{WY_{ij}} = \mathrm{P_i} - \mathrm{AET_i} \tag{5}$$

$$\mathrm{AET_i} = \mathrm{P_i} \times \left(\frac{1 + \mathrm{w_i R_{ij}}}{1 + \mathrm{w_i R_{ij}} + \frac{1}{\mathrm{R_{ij}}}} \right) \tag{6}$$

where $\mathrm{WR_{ij}}$ is the annual WR of land use type j on pixel i, mm; $\mathrm{WY_{ij}}$ is the annual water yield, mm; $\mathrm{RF_{ij}}$ is the annual surface runoff, mm; $\mathrm{P_i}$ is the annual precipitation, mm; C_{ij} is the average surface runoff coefficient of land use type j on pixel i; $\mathrm{AET_i}$ is the annual actual evapotranspiration, mm; w_i is a non-physical parameter characterizing natural climate and soil properties, dimensionless; R_{ij} is the Budyko Dryness Index, dimensionless.

Supplementary Table 2. WR coefficient.

lucode	**LULC_desc**	K_c[8]	***root_depth***[8]	***LULC_veg***	C_{ij}[9]
1	Cultivated land	0.6	1000	1	0.347
2	Forest	1	7000	1	0.0267
3	Grassland	0.65	1500	1	0.0937
4	Water area	1	1000	0	0
5	Built-up area	0.3	500	0	1
6	Unused land	0.2	10	0	1

Note: K_c is the evapotranspiration coefficient; *root_depth* is the maximum root depth; *LULC_veg* refers to the presence or absence of vegetation. 1 indicates the presence of vegetation and 0 indicates the absence of vegetation.

Heat Mitigation. We applied the InVEST Urban Cooling module to calculate HM. The module calculates the cooling capacity (CC_i) of the pixel i based on shade, evapotranspiration (ETI_i), albedo, and distance to cold islands such as parks. If pixel i is unaffected by any large green spaces (more than 2 hectares), HM is equal to CC_i, otherwise equal to a distance-weighted average of the CC_i from the large green spaces and the pixel i. The calculation formula are as follows.

$$\mathrm{CC_i} = 0.6 \times \mathrm{shade_i} + 0.2 \times \mathrm{ETI_i} + 0.2 \times \mathrm{albedo_i} \tag{7}$$

$$\mathrm{ETI_i} = \frac{\mathrm{K_c} \times \mathrm{ET_0}}{\mathrm{ET_{max}}} \tag{8}$$

$$\mathrm{GA_i} = \mathrm{pixel_{area}} \times \sum_{\mathrm{j \in d\ radius\ from\ i}} \mathrm{g_j} \tag{9}$$

$$\mathrm{CC_{parki}} = \sum_{\mathrm{j \in d\ radius\ from\ i}} \mathrm{g_j} \times \mathrm{CC_j} \times \mathrm{e}^{\left(\frac{-\mathrm{d(i,j)}}{\mathrm{d_{cool}}}\right)} \tag{10}$$

$$\mathrm{HM_i} = \begin{cases} \mathrm{CC_i}, & \text{if } \mathrm{CC_i} \geq \mathrm{CC_{parki}} \text{ or } \mathrm{CA_i} < 2\mathrm{ha} \\ \mathrm{CC_{parki}}, & \text{otherwise} \end{cases} \tag{11}$$

where HM_i is the HM on pixel i; CC_i is the cooling capacity on pixel i. Its value is comprised between 0 and 1. 1 indicates maximum cooling capacity, 0 indicates no cooling capacity. ET_0 is the potential evapotranspiration, mm; ET_{max} is the maximum value of ET_0; $pixel_{area}$ is the area of a pixel in ha; CC_{parki} is the cooling capacity of each park; d(i, j) is the distance between pixel i and pixel j; d_{cool} is the distance for which a green space has a cooling effect.

Supplementary Table 3. HM coefficient.

lucode	LULC_desc	*shade*[10]	K_c	*albedo*[11]	g_j[10]
1	Cultivated land	0	0.6	0.2	1
2	Forest	1	1	0.2	1
3	Grassland	0	0.65	0.2	1
4	Water area	0	1	0.05	1
5	Built-up area	0	0.3	0.15	0
6	Unused land	0	0.2	0.25	0

Note: *shade* refers to the ability of trees to provide shade. 1 indicates that it can provide shade, and 0 indicates that it cannot provide shade; *albedo* is the proportion of reflected solar radiation, with values between 0 and 1, 0 indicates the maximum absorption, and 1 indicates the maximum reflectivity; g_j indicates whether it can be regarded as a green space, 0 indicates that it cannot be regarded as a green space, and 1 indicates that it can be regarded as a green space; $albedo_i$ refers to the study of Stewart et al.[11], and $shade_i$ and g_j refers to the study of Zawadzka et al[10].

Flood Mitigation. In the study, the Urban Flood Risk Mitigation module of the InVEST model was used to calculate FM. The module estimates runoff using SCS-Curve Number.The calculation formula are as follows.

$$\mathrm{FM_i} = 1 - \frac{\mathrm{R_i}}{\mathrm{P_{max}}} \tag{12}$$

$$\mathrm{R_i} = \begin{cases} \dfrac{(\mathrm{P} - 0.2\mathrm{I_i})^2}{\mathrm{P} + 0.8\mathrm{I_i}}, & \mathrm{P} > 0.2\mathrm{I_i} \\ 0, & \mathrm{P} \le 0.2\mathrm{I_i} \end{cases} \tag{13}$$

$$\mathrm{I_i} = \frac{25400}{\mathrm{CN_i}} - 254 \tag{14}$$

Among them, FM_i is the annual FM of pixel i, dimensionless, with values between 0 and 1; P_{max} is the design storm depth, mm; R_i is runoff, mm; I_i is the potential retention, mm.

Supplementary Table 4. FM coefficient.

lucode	**LULC_desc**	***CN_A***	***CN_B***	***CN_C***	***CN_D***
1	Cultivated land	54	70	80	84
2	Forest	36	60	73	79
3	Grassland	49	69	79	84
4	Water area	0	0	0	0
5	Built-up area	85	90	92	94
6	Unused land	77	86	91	94

Note: *CN* is the runoff curve value of pixel i, dimensionless. The value range of *CN* is between 0 ~ 100. *CN* equal to 100 indicates that rainfall is completely converted to runoff. We refer to the data from the US Department of Agriculture[12].

We found that the Urban Flood Risk Mitigation module mainly affects the value of each pixel based on changes in land type and soil characteristics. In the process of urbanization, the original natural open soil in the core area has been transformed into artificial surface, building and other closed soil, and its soil physical and chemical properties will change significantly. However, due to the huge workload of soil survey, the Harmonized World Soil Database is widely recognized and used in relevant research in China[13]. Therefore, the FM simulated by the InVEST model in this study is mainly determined by the LULC from 1990 to 2020. Although the SCS-Curve method used in the module could well reflect the ranking of FM on different land uses, we found that for the areas where the land type has not changed for many years, the FM obtained by the module is basically consistent. Vegetation loss caused by human activities such as agricultural production, deforestation and settlement is also prone to flooding[14]. Many studies use NDVI to measure vegetation coverage in study areas[15] and to detect flood events[16]. These findings indicate that the higher the NDVI value, the lower the possibility of flooding[17,18]. Therefore, we tried to use NDVI to correct the Urban Flood Risk Mitigation module, and use the corrected calculation results to participate in the analysis. The correction formula is as follows.

$$\mathrm{FMC_i} = \mathrm{NDVI_i} \times \mathrm{FM_i} \tag{15}$$

Among them: $\mathrm{FMC_i}$ is the corrected $\mathrm{FM_i}$. $\mathrm{NDVI_i}$ is the *NDVI* value of pixel i, *NDVI*$\in$[-1, 1]. *NDVI* greater than 0 indicates vegetation coverage, and the value of *NDVI* increases with the increase of vegetation coverage Areas with *NDVI* close to 0 are mainly impervious surfaces. Areas with *NDVI* less than 0 are mainly water area. This study sets water area to not provide FM. Therefore, replace the negative value with 0, which is $0 \le \mathrm{NDVI_i} \le 1$.

Supplementary Method 2

The formulas for the Theil-Sen median trend analysis and the Mann-Kendall test are as follows.

$$\beta = \mathrm{median}\left(\frac{\mathrm{ES_y} - \mathrm{ES_x}}{\mathrm{y} - \mathrm{x}}\right), \forall \mathrm{y} > \mathrm{x} \tag{16}$$

Among them: β is the change trend of ES. β > 0 indicates that ES is on an increasing trend, and β < 0 indicates that ES is on a downward trend. $\mathrm{ES_y}$ and $\mathrm{ES_x}$ are time series data of ES; y and x are time series.

$$\mathrm{S} = \sum_{\mathrm{x}}^{N-1} \sum_{\mathrm{y=x+1}}^{N} \mathrm{sgn}(\mathrm{ES_y} - \mathrm{ES_x}) \tag{17}$$

$$\mathrm{sgn}(\mathrm{ES_y} - \mathrm{ES_x}) = \begin{cases} 1\ , \mathrm{ES_y} - \mathrm{ES_x} > 0 \\ 0\ , \mathrm{ES_y} - \mathrm{ES_x} = 0 \\ -1, \mathrm{ES_y} - \mathrm{ES_x} < 0 \end{cases} \tag{18}$$

$$\mathrm{Var(S)} = \frac{N(N-1)(2N+5)}{18} \tag{19}$$

$$\mathrm{Z} = \begin{cases} \frac{\mathrm{S}}{\sqrt{\mathrm{Var(S)}}}, \mathrm{S} > 0 \\ 0\quad, \mathrm{S} = 0 \\ \frac{\mathrm{S}+1}{\sqrt{\mathrm{Var(S)}}}, \mathrm{S} < 0 \end{cases} \tag{20}$$

Where, S is the test statistic; *N* is the length of the time series, i.e. *N* = 31; Z is the normalized test statistic. Referring to the division method of Shah et al.[19], when |Z| is greater than 1.65, 1.96 and 2.58, it means that the trend analysis has passed the significance tests of 90 %, 95 % and 99 % reliability, respectively.

Supplementary Table 5. Trend characteristics of ESs[19].

β	Z	Trend features of ESs	Trend types of ESs
$\beta > 0$	$\lvert Z\rvert > 2.58$	Extremely significant increase	Increase***
	$1.96 < \lvert Z\rvert \le 2.58$	Significant increase	Increase**
	$1.65 < \lvert Z\rvert \le 1.96$	Sub-significant increase	Increase*
	$\lvert Z\rvert \le 1.65$	Weak increase	Increase
$\beta = 0$	$\lvert Z\rvert$	No change	No change
$\beta < 0$	$\lvert Z\rvert \le 1.65$	Weak decrease	Decrease
	$1.65 < \lvert Z\rvert \le 1.96$	Sub-significant decrease	Decrease*
	$1.96 < \lvert Z\rvert \le 2.58$	Significant decrease	Decrease**
	$\lvert Z\rvert > 2.58$	Extremely significant decrease	Decrease***

Codes used in Matlab for analyzing spatial-temporal change of ESs are as follows.

```
clear
[a,R]=geotiffread('E:\Tool\Matlab\MK_Sen\WR_2020.tif');
info=geotiffinfo('E:\Tool\Matlab\MK_Sen\WR_2020.tif');
[m,n]=size(a);
cd=2020-1990+1;
datasum=zeros(m*n,cd)+0;
p=1;
for year=1990:2020
    filename=['E:\Tool\Matlab\MK_Sen\WR_',int2str(year),'.tif'];
    data=importdata(filename);
    data=reshape(data,m*n,1);
    datasum(:,p)=data;
    p=p+1;
end
sresult=zeros(m,n);
result=zeros(m,n);
for i=1:size(datasum,1)
    data=datasum(i,:);
    if min(data)>0
        sgnsum=[];
        for k=2:cd
            for j=1:(k-1)
                sgn=data(k)-data(j);
                if sgn>0
                    sgn=1;
                else
                    if sgn<0
                        sgn=-1;
                    else
                        sgn=0;
                    end
                end
                sgnsum=[sgnsum;sgn];
            end
        end
        add=sum(sgnsum);
        sresult(i)=add;
    end
end
for i=1:size(datasum,1)
    data=datasum(i,:);
    if min(data)>0
```

```
            valuesum=[];
            for k1=2:cd
                for k2=1:(k1-1)
                    cz=data(k1)-data(k2);
                    jl=k1-k2;
                    value=cz./jl;
                    valuesum=[valuesum;value];
                end
            end
            value=median(valuesum);
            result(i)=value;
        end
end

vars=cd*(cd-1)*(2*cd+5)/18;
zc=zeros(m,n);
sy=find(sresult==0);
zc(sy)=0;
sy=find(sresult>0);
zc(sy)=(sresult(sy)-1)./sqrt(vars);
sy=find(sresult<0);
zc(sy)=(sresult(sy)+1)./sqrt(vars);

result1=reshape(result,m*n,1);
zc1=reshape(zc,m*n,1);
tread=zeros(m,n);
for i=1:size(datasum,1)
        %result1(i)
        if result1(i)>0
            if abs(zc1(i))>=2.58
                tread(i)=4;
            elseif (1.96<=abs(zc1(i)))&&(abs(zc1(i))<2.58)
                tread(i)=3;
            elseif (1.645<=abs(zc1(i)))&&(abs(zc1(i))<1.96)
                tread(i)=2;
            else
                tread(i)=1;
            end
            elseif result1(i)<0
            if abs(zc1(i))>=2.58
                tread(i)=-4;
            elseif (1.96<=abs(zc1(i)))&&(abs(zc1(i))<2.58)
                tread(i)=-3;
            elseif (1.645<=abs(zc1(i)))&&(abs(zc1(i))<1.96)
```

```
            tread(i)=-2;
        else
            tread(i)=-1;
        end
        else
            tread(i)=0;
    end
end
geotiffwrite('E:\Tool\Matlab\MK_Sen\WR_CASA\NPPtread.tif',tread,R,'GeoKeyDirectoryTag',info.GeoTIFFTags.GeoKeyDirectoryTag)
```

Supplementary Method 3

The PLUS model is available from https://github.com/HPSCIL/Patchgenerating_Land_Use_Simulation_Model (accessed 15 March 2024). Firstly, a total of 12 categories of drivers were selected, including average annual temperature, average annual precipitation, DEM, slope, GDP, population, distance from rivers, distance from lakes, distance from railway, distance from highway, distance from settlements, soil type, using the LEAS module to identify its driving force. Then, to test the effectiveness of the simulation results, we used the year 2000 as the initial year to simulate the land demand in 2020 and then compared it with the actual areas of each land use type in 2020. The result shows that the simulation results are scientifically reliable, with a kappa coefficient of 0.883 and an overall accuracy of 0.923. Subsequently, this study continued to simulate the land use in the future under multi-scenarios. Three alternative potential land use change scenarios were developed, namely, business as usual (BAU), cropland protection (CP), and ecological conservation (EC), to detect the ES changes and interactions under these scenarios. Te principles and goals of designing these scenarios were as follows:

BAU scenario. This scenario assumed that the historical land use change trends are maintained; the land demand in the period of 2025–2050 can be calculated according to the initial transition probability matrix for the period of 2010 ~ 2020.

CP scenario. This scenario highlights the principles of national food security. To achieve this, the transfer probability of cropland to built-up land and unused land was reduced by 40% compared to BAU; the transfer probability of cropland to forest, grassland and water area was reduced by 10% compared to BAU; and these were added to cropland. And permanent basic cropland as constrained zones.

EC scenario. This scenario described a situation in which the local government strengthens the protection of forest, grassland, and water. Similar to the CP scenario, we calculated the land demands for this scenario by modifying the conversion rate between certain land use types. In the period of 2025 ~ 2050, the conversion probability of cropland to built-up land and unused land was reduced by 40% compared to BAU, and this was added to cropland; the conversion probability of forest, grassland, and water into cropland, built-up area and unused land decrease by 40%, and this was added to forest, grassland, and water; the conversion probability of forest into grassland and waters decrease by 20%. And ecological protection red line as constrained zones.

In addition, urban development scenario was not considered in this study. Data from the China Urban Statistics Yearbook 2021 (http://www.stats.gov.cn/sj/) show that the urbanization rate for Suzhou, Wuxi and Changzhou is 81.7%, 82.8% and 77.1% , respectively. It can be seen that the Su-Xi-Chang region has already reached a high urban development level and does not need to set an urban development scenario for the next 30 years.

Supplementary Table 6. Conversion cost matrix used for simulating different land use scenarios.

Scenarios	LULC_desc	Cultivated land	Forest	Grassland	Water area	Built-up area	Unused land
BAU scenario	Cultivated land	1	1	1	1	1	1
	Forest	1	1	1	1	1	1
	Grassland	1	1	1	1	1	1
	Water area	1	1	1	1	1	1
	Built-up area	1	0	0	1	1	0
	Unused land	1	1	1	1	1	1
CP scenario	Cultivated land	1	0	0	0	0	0
	Forest	1	1	1	1	1	1
	Grassland	1	1	1	1	1	1
	Water area	1	1	1	1	1	1
	Built-up area	1	0	0	1	1	0
	Unused land	1	1	1	1	1	1
EC scenario	Cultivated land	1	1	1	1	1	0
	Forest	0	1	1	1	0	0
	Grassland	0	1	1	1	0	0
	Water area	0	1	1	1	1	0
	Built-up area	1	1	1	1	1	0
	Unused land	1	1	1	1	1	1

Note: the conversion cost defines whether a conversion from one land use type (in the columns) to another (in the rows) is possible. A value of 0 denotes that the conversion is not allowed, and a value of 1 denotes that the conversion is possible.

Supplementary Table 7. The neighborhood weights for individual land use type under the different scenarios.

Scenarios	Cultivated land	Forest	Grassland	Water area	Built-up area	Unused land
BAU scenario	0.524	0.468	0.496	0.1	1	0.497
CP scenario	1	0.468	0.496	0.1	1	0.1
EC scenario	0.2	1	0.9	0.6	0.4	0.1

Note: The domain weights occurred within the 0 ~ 1 range, and higher values indicate a higher expansion intensity of the land use type.

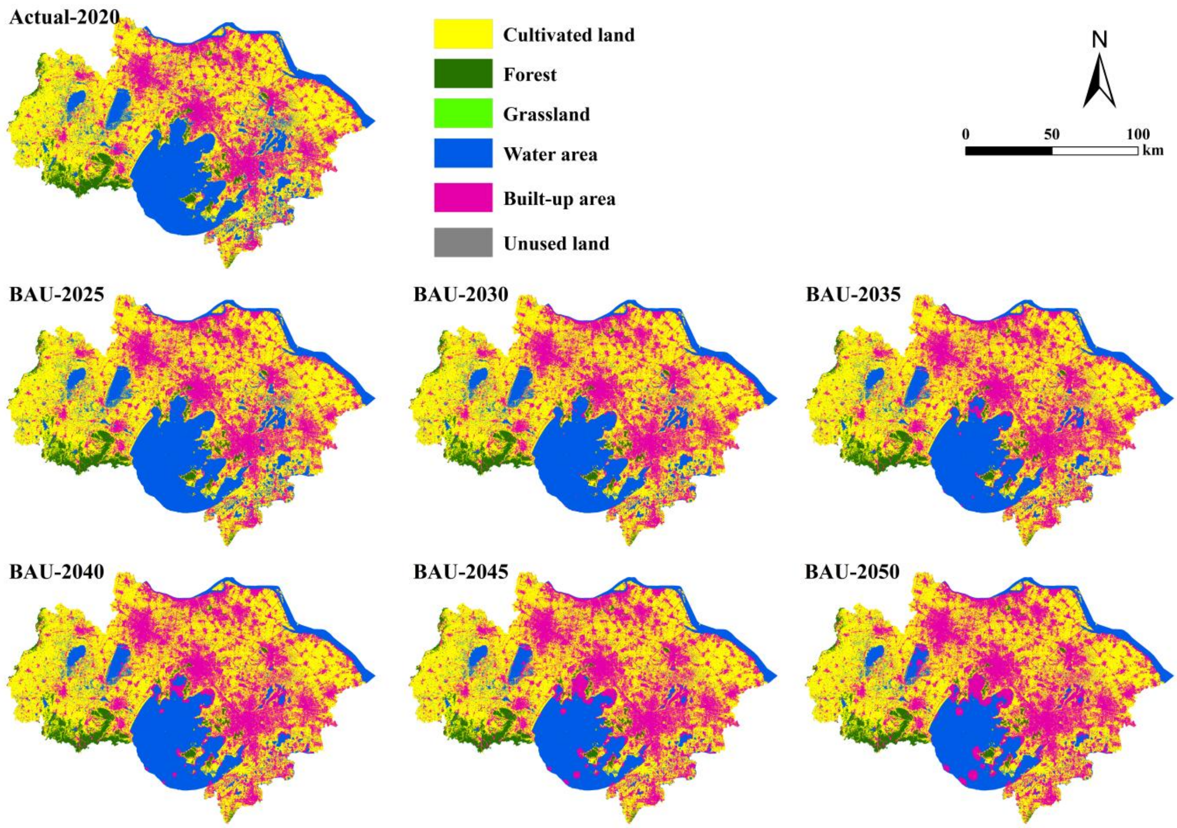

Supplementary Figure 3. The simulated land use pattern under BAU scenario from 2025 to 2050.

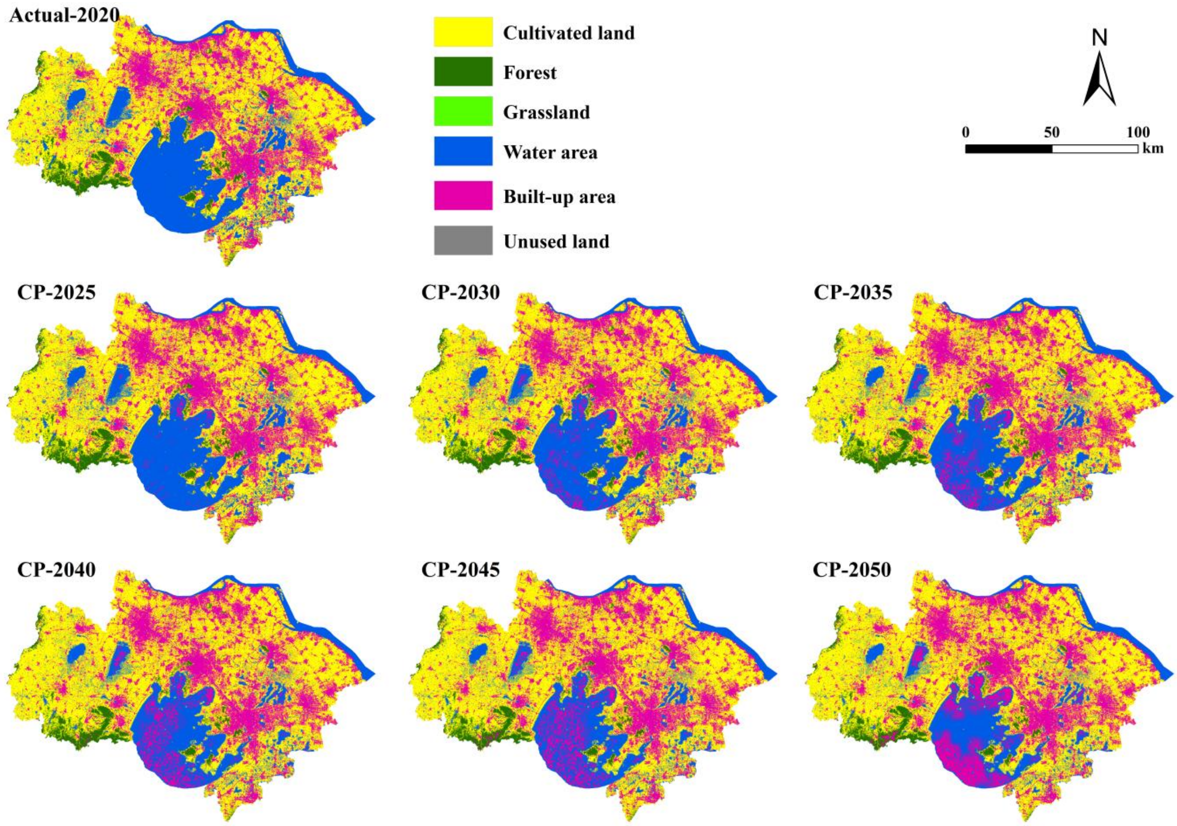

Supplementary Figure 4. The simulated land use pattern under CP scenario from 2025 to 2050.

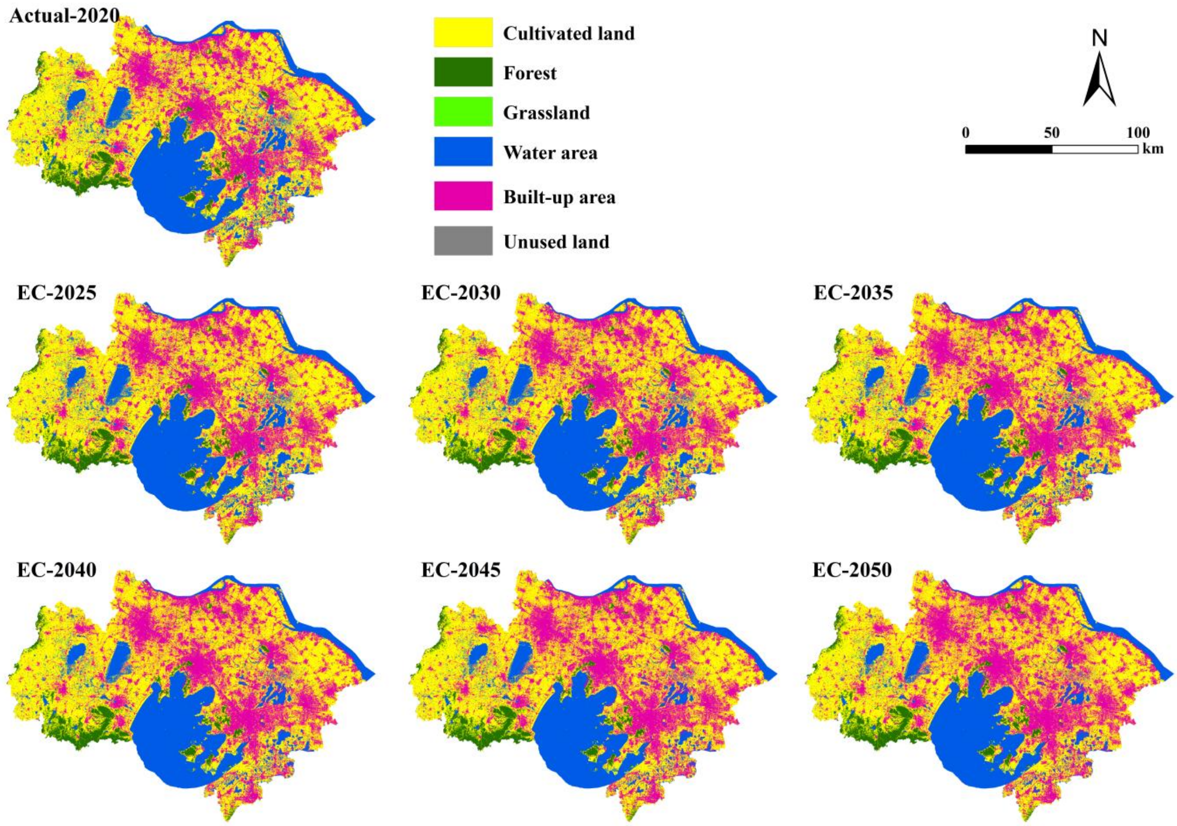

Supplementary Figure 5. The simulated land use pattern under EC scenario from 2025 to 2050.

Supplementary Table

Supplementary Table 8. Data used in this study.

Data Name	Data Type	Year	Source
LULC	30 m × 30 m Raster data	1990 ~ 2020	30 m annual land cover and its dynamics in China from 1990 to 2019 (Version 1.0.0)[20]. (https://doi.org/10.5281/zenodo.4417810 accessed on 6 October 2022)
Total population	1 km × 1 km Raster data	1990, 2000, 2010, 2019	Resource and Environment Science and Data Center. (https://www.resdc.cn/DataList.aspx accessed on 5 October 2022)
Nighttime light imagery	1 km × 1 km Raster data	1992 ~ 2020	An improved time-series DMSP-OLS-like data (1992 ~ 2021) in China by integrating DMSP-OLS and SNPP-VIIRS - Harvard Dataverse. (https://dataverse.harvard.edu/dataset.xhtml?persistentId=doi:10.7910/DVN/GIYGJU/ accessed on 10 October 2022)
Normalized difference vegetation index	30 m × 30 m Raster data	1990 ~ 2020	Resource and Environment Science and Data Center. (https://www.resdc.cn/DataList.aspx accessed on 8 October 2022)
Total crop production	Whole study area Statistical data	1990 ~ 2020	Statistical yearbook of CNKI. (https://data.cnki.net/Yearbook accessed on 7 October 2022)
Average precipitation	1 km × 1 km Raster data	1990 ~ 2020	National Earth System Science Data Center. (http://www.geodata.cn accessed on 6 October 2022)
Average temperature	1 km × 1 km Raster data	2020	National Earth System Science Data Center. (http://www.geodata.cn accessed on 6 October 2022)
Potential evapotranspiration	1 km × 1 km Raster data	1990 ~ 2020	National Earth System Science Data Center. (http://www.geodata.cn accessed on 6 October 2022)
Soil depth, sand, silt, clay, soil organic matter content	1 km × 1 km Raster data	1995	Agriculture Organization of United Nations. (https://www.fao.org/soils-portal/data-hub/soil-maps-and-databases/harmonized-world-soil-database-v12 accessed on 1 October 2022)
Hydrologic soil groups	250 m × 250 m Raster data	2015	Global Hydrologic Soil Groups for Curve Number-Based Runoff. Modeling (https://daac.ornl.gov/ accessed on 18 October 2022)
Soil type	1 km × 1 km Raster data	1995	Resource and Environment Science and Data Center. (https://www.resdc.cn/Default.aspx accessed on 4 March 2024)
DEM	30 m × 30 m Raster data	2020	Geospatial Data Cloud. (http://www.gscloud.cn/search accessed on 5 March 2024)
Slope	30 m × 30 m Raster data	2020	Obtained by DEM processing in ArcMap10.8 software.
GDP	1 km × 1 km Raster data	2019	Resource and Environment Science and Data Center. (https://www.resdc.cn/Default.aspx accessed on 4 March 2024)
Distance to rivers	30 m × 30 m Raster data	2021	National Catalogue Service For Geographic Information. (https://www.webmap.cn/main.do?method=index accessed on 7 March 2024)
Distance to lakes	30 m × 30 m Raster data	2021	National Catalogue Service For Geographic Information. (https://www.webmap.cn/main.do?method=index accessed on 7 March 2024)
Distance to railway	30 m × 30 m	2021	National Catalogue Service For Geographic Information.

	Raster data		(https://www.webmap.cn/main.do?method=index accessed on 7 March 2024)
Distance to highway	30 m × 30 m Raster data	2021	National Catalogue Service For Geographic Information. (https://www.webmap.cn/main.do?method=index accessed on 7 March 2024)
Distance to settlements	30 m × 30 m Raster data	2021	National Catalogue Service For Geographic Information. (https://www.webmap.cn/main.do?method=index accessed on 7 March 2024)
Ecological protection red line	30 m × 30 m Raster data	2021	Municipal Natural Resources Office.
permanent basic cropland	30 m × 30 m Raster data	2021	Municipal Natural Resources Office.

Supplementary Figure

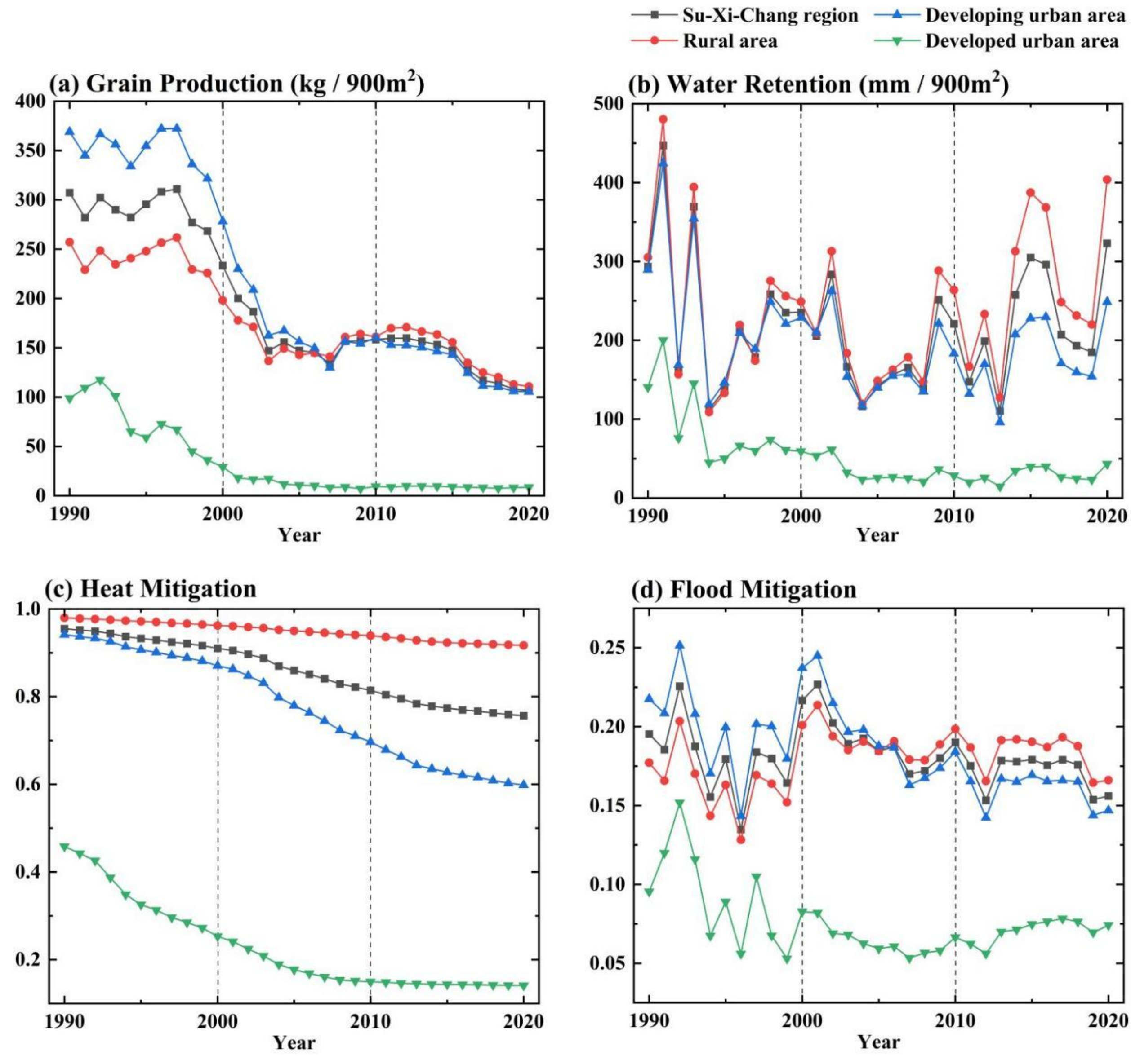

Supplementary Figure 6. Temporal change trend of ESs in the whole study area during 1990 ~ 2020 (No smoothing). (a) grain production; (b) water retention; (c) heat mitigation; (d) flood mitigation.

Supplementary References

[1] Xu, X. *et al.*, Impacts of land use changes on net ecosystem production in the Taihu Lake Basin of China from 1985 to 2010. *J GEOPHYS RES-BIOGEO* **122** 690-707 (2017).

[2] Xu, Y., Cheng, X. & Gun, Z., What Drive Regional Changes in the Number and Surface Area of Lakes Across the Yangtze River Basin During 2000–2019: Human or Climatic Factors? *Water Resources Research* **58** 616 (2022).

[3] Naser, M. A., Khosla, R., Longchamps, L. & Dahal, S., Using NDVI to Differentiate Wheat Genotypes Productivity Under Dryland and Irrigated Conditions. *Remote Sens* **12** 824 (2020).

[4] ANDRADE, T. G., ANDRADE JUNIOR, A. S. D., SOUZA, M. O., LOPES, J. W. B. & VIEIRA, P. F. D. M., SOYBEAN YIELD PREDICTION USING REMOTE SENSING IN SOUTHWESTERN PIAUÍ STATE, BRAZIL. *REV CAATINGA* **35** 105-116 (2022).

[5] Onwuchekwa-Henry, C. B., Ogtrop, F. V., Roche, R. & Tan, D. K. Y., Model for Predicting Rice Yield from Reflectance Index and Weather Variables in Lowland Rice Fields. *Agriculture* **12** 130 (2022).

[6] Liu, W. *et al.*, The tradeoffs between food supply and demand from the perspective of ecosystem service flows: A case study in the Pearl River Delta, China. *J. Environ Manage* **301** 113814 (2022).

[7] Bai, Y., Ochuodho, T. O. & Yang, J., Impact of land use and climate change on water-related ecosystem services in Kentucky, USA. *Ecol Indic* **102** 51-64 (2019).

[8] Bai, Y., Chen, Y., Alatalo, J. M., Yang, Z. & Jiang, B., Scale effects on the relationships between land characteristics and ecosystem services- a case study in Taihu Lake Basin, China. *Sci Total Environ* **716** 137083 (2020).

[9] Ministry of Ecology and Environment of the People's Republic of China. Guidelines for the Delineation of Ecological Protection Red Lines. https://www.mee.gov.cn/gkml/hbb/bgt/201707/W020170728397753220005.pdf (2017).

[10] Zawadzka, J. E., Harris, J. A. & Corstanje, R., Assessment of heat mitigation capacity of urban greenspaces with the use of InVEST urban cooling model, verified with day-time land surface temperature data. *Landscape Urban Plan* **214** 104163 (2021).

[11] STEWART, I. D. & OKE, T. R., LOCAL CLIMATE ZONES FOR URBAN TEMPERATURE STUDIES. *B AM METEOROL SOC* **93** 1879-1900 (2012).

[12] U. S. Department Of Agriculture, S. C. S. E., Urban hydrology for small watersheds. *Technical Release - United States Department of Agriculture. Soil Conservation Service, Engineering Division* 5 (1975).

[13] Zhang, H., Deng, W., Zhang, S., Peng, L. & Liu, Y., Impacts of urbanization on ecosystem services in the Chengdu-Chongqing Urban Agglomeration: Changes and trade-offs. *Ecol Indic* **139** 108920 (2022).

[14] Mind'Je, R. *et al.*, Flood susceptibility modeling and hazard perception in Rwanda. *Int J Disaster Risk Reduct* **38** 101211 (2019).

[15] Parizi, E., Bagheri-Gavkosh, M., Hosseini, S. M. & Geravand, F., Linkage of geographically weighted regression with spatial cluster analyses for regionalization of flood peak discharges drivers: Case studies across Iran. *J CLEAN PROD* **310** 127526 (2021).

[16] Shrestha, R. *et al.*, Regression model to estimate flood impact on corn yield using MODIS NDVI and USDA cropland data layer. J Integr Agric **16** 398-407 (2017).

[17] Tien Bui, D. *et al.*, A novel deep learning neural network approach for predicting flash flood susceptibility: A case study at a high frequency tropical storm area. *Sci Total Environ* **701** 134413 (2020).

[18] Kim, H. Y., Analyzing green space as a flooding mitigation - storm Chaba case in South Korea. *GEOMAT NAT HAZ RISK* **12** 1181-1194 (2021).

[19] Shah, S. A., Jehanzaib, M., Kim, M. J., Kwak, D. & Kim, T., Spatial and Temporal Variation of Annual and Categorized Precipitation in the Han River Basin, South Korea. *KSCE J CIV ENG* **26** 1990-2001 (2022).

[20] Yang, J. & Huang, X., The 30 m annual land cover dataset and its dynamics in China from 1990 to 2019. *EARTH SYST SCI DATA* **13** 3907 (2021).